DOI: 10.1002/chem.200800240

Pillaring of $CdCl_2$-Like Layers in Lanthanide Metal–Organic Frameworks: Synthesis, Structure, and Photophysical Properties

Partha Mahata, K. V. Ramya, and Srinivasan Natarajan*[a]

Abstract: A hydrothermal reaction of lanthanide salts, pyridine-2,3-dicarboxylic acid, benzene-1,4-dicarboxylic acid, and water gave rise to a new series of three-dimensional mixed carboxylates (homocyclic and heterocyclic) of lanthanides with the general formula $[M_2(H_2O)_4][\{C_5H_3N(COO)_2\}_2\{C_6H_4(COO)_2\}]$, M = La (**I**), Pr (**II**), and Nd (**III**). The structure consists of $M_2O_{14}N_2$ dimeric units connected by pyridine-2,3-dicarboxylate moieties to form two-dimensional layers that are pillared by terephthalate units. The structures also possess two coordinated water molecules, which are arranged to form one-dimensional helical chains and can be reversibly adsorbed. The connectivity within the layers closely resembles that of the $CdCl_2$ layered structure with 3^6 topology. To the best of our knowledge, this is the first observation of $CdCl_2$ topology in lanthanide metal–organic framework compounds. Partial substitution of La^{3+} in **I** by Eu^{3+} and Tb^{3+} (2 and 4%) gives rise to characteristic red/pink or green emission, which suggests a ligand-sensitized metal-centered emission. The Nd compound **III** shows interesting UV and blue emission through an up-conversion process.

Keywords: carboxylate ligands · hydrothermal synthesis · lanthanides · luminescence · metal–organic frameworks

Introduction

Research in the field of metal–organic frameworks (MOFs) continues to be exciting for the many potential applications in the areas of sorption, separation, and other related properties.[1] Multidimensional infinite MOF structures have been obtained by a careful combination of the geometrical preferences of the metal ion and the functionalities of the organic ligands through rational design.[2] Many of these compounds are based on transition elements. The design and synthesis of lanthanide-based MOFs, on the other hand, may be more difficult due to the high and varied coordination requirements of the lanthanide ions.[3] It has been well established that lanthanide ions have a higher affinity for hard donor ligands, such as the O-donor ligands.[4] This inherent preference of the lanthanide ions has been utilized for the preparation of many multi-carboxylates of different dimensionalities.[5]

The complex connectivities observed in some of the MOF structures prompted researchers to visualize them as simple topologies based on well-known networks. Topological descriptions, of course, have been traditionally used for the understanding of the three-dimensional structures of aluminosilicate zeolites and related materials.[6] In this approach, the three-dimensionally extended structures are simplified by considering connectivities based on linked two-dimensional layers. The two-dimensional layers, in turn, are described as networked topologies derived from hexagons, squares, and triangles.[7] These units can combine either individually or in association, thus giving rise to a variety of two-dimensional nets. The most well established and the simplest of the two-dimensional nets are the 6^3 (three hexagons connected at a node), 4^4 (four squares connected at a node), and 3^6 (six triangles connected at a node) topologies. These are the Schläfli notations, and well-known examples of such nets are graphite and corundum (6^3), face-centered cubic structures (4^4), and the $CdCl_2$ structure (3^6).[7]

An examination of the available literature on MOF structures indicates that the 6^3 and 4^4 topologies are more common[8,9] than the 3^6 topology. The first 3^6 topology was observed and described by Schröder and co-workers in $[Zn_3(1,4\text{-dbc})_3(def)_2]\cdot DEF$ (1,4-bdc: 1,4-benzenedicarboxylate,

[a] P. Mahata, K. V. Ramya, Prof. Dr. S. Natarajan
Framework Solids Laboratory
Solid State and Structural Chemistry Unit
Indian Institute of Science
Bangalore-560012 (India)
Fax: (+91) 80-2360-1310
E-mail: snatarajan@sscu.iisc.ernet.in

Supporting information for this article is available on the WWW under http://www.chemeurj.org/ or from the author.

terephthalate; def: diethylformamide).[10] Subsequently, the 3^6 topology was observed for $[\{Cu_3(\mu_3\text{-}OH)\}_2(\mu_3\text{-}btr)_6(\mu_4\text{-}btr)(\mu\text{-}X)X_4]X_5{\cdot}n\,H_2O$ (X = Br, $n = 6$; X = Cl, $n = 8$; btr: 4,4′-bis(1,2,4-triazole)), which possesses a two-dimensional structure.[11] Recently, a simple (4,4) connectivity has also been discussed in terms of 3^6 topology by considering hydrogen-bond interactions in $[M(btza)_2(H_2O)_2]{\cdot}2\,H_2O$ (M = Mn, Zn; btza: bis(1,2,4-triazol-1-yl)acetate).[12]

We have been interested in the study of lanthanide compounds due to their interesting optical behavior arising from the ligand-sensitized and sharp f–f emissions. In addition, the higher coordination requirement of lanthanides can be gainfully utilized to give rise to interesting network topologies. Among the lanthanide ions, Eu^{3+} and Nd^{3+} are important as they can be used in the visible region ($\lambda = 500$–700 nm) and in the near-IR region ($\lambda = 800$–1700 nm), respectively. In addition, Nd^{3+} compounds also show up-conversion behavior by converting the IR radiation into the visible region by a two-photon absorption process.[13]

A detailed literature search indicated that the lanthanide carboxylates are formed with either homocyclic (benzene carboxylates)[14] or heterocyclic systems (such as pyridine, imidazole carboxylates).[15] There are not many reports of investigations on the formation of lanthanide MOFs using hybrid aromatic carboxylates (homocyclic and heterocyclic).[16]

We sought to investigate the formation of new lanthanide carboxylates employing hetero (quinolinic acid) and homo (terephthalic acid) aromatic dicarboxylic acids. Herein, we describe the successful preparation of a new series of MOF compounds of lanthanides with the general formula $[M_2(H_2O)_4][\{C_5H_3N(COO)_2\}_2\{C_6H_4(COO)_2\}]$, M = La (**I**), Pr (**II**), and Nd (**III**). Of these, only **I** was obtained as good-quality single crystals, whereas **II** and **III** were formed as pure polycrystalline powder samples. In addition, we also prepared samples doped with Eu^{3+} (2 and 4 mol%) and Tb^{3+} (2 and 4 mol%) in place of La^{3+} (**I**). The structures of all the compounds are similar and are formed by a network of M^{3+} ions and quinolinate units, which give rise to a two-dimensional layered structure that resembles the $CdCl_2$ topology (3^6). This is the first observation of $CdCl_2$ topology, to the best of our knowledge, in a lanthanide carboxylate system. The lanthanide–quinolinate layers are pillared by terephthalate units, thus completing the three-dimensional structure. Optical studies indicate metal-centered emission in the doped compounds and an interesting UV and blue emission through a two-photon up-conversion process in **III**. Herein, we describe the synthesis, structure, and photophysical and related properties of all the compounds.

Results and Discussion

Structure: Compound **I** has 21 non-hydrogen atoms in the asymmetric unit, in which one La^{3+} ion, one pyridine-2,3-dicarboxylate (quinolinate) anion, half a benzene-1,4-dicarboxylate (terephthalate) anion, and two water molecules are present (see Figure S1 in the Supporting Information). The metal atom, La(1), is surrounded by eight oxygen atoms and one nitrogen atom and has a distorted tricapped trigonal prismatic environment ($La(1)O_8N$, CN = 9; see Figure S1 in the Supporting Information). Of the eight oxygen atoms, two [O(5), O(6)] are coordinated water molecules and the nitrogen atom is part of the pyridine ring. Of the six remaining oxygen atoms, four are from the pyridine dicarboxylate units and two are from the benzene dicarboxylate units. One oxygen atom, O(1), has μ_3 connectivity linking two metal centers and a carbon atom. The La–O bonds have lengths in the range 2.505(2)–2.674(2) Å and the La–N bond has a length of 2.834(3) Å. The O/N-La-O/N bond angles are in the range 49.94(7)–157.53(7)°. The coordination around the La^{3+} ions was based on assuming typical La–O distances in the range 2.4–2.8 Å. The selected bond lengths are listed in Table 1.

Table 1. Selected bond lengths [Å] observed in $[La_2(H_2O)_4][\{C_5H_3N(COO)_2\}_2\{C_6H_4(COO)_2\}]$ (**I**).

Bond[a]	Amplitude	Bond	Amplitude
La(1)–O(1)	2.505(2)	La(1)–O(5)	2.604(2)
La(1)–O(2)#1	2.511(2)	La(1)–O(6)	2.610(2)
La(1)–O(3)#2	2.516(2)	La(1)–O(7)	2.674(2)
La(1)–O(4)	2.527(2)	La(1)–N(1)	2.834(3)
La(1)–O(1)#3	2.604(2)		

[a] Symmetry transformations used to generate equivalent atoms: #1: x, $-y+3/2$, $z+1/2$; #2: x, $y-1$, z; #3: $-x+1$, $-y+1$, $-z+1$.

The three-dimensional structure can be explained by considering simpler building units. Thus, the $La(1)O_8N$ polyhedral units are connected through a common edge with another La(1) atom by two μ_3-coordinated oxygen atoms [O(1)] to form a dimer of the formula $La_2O_{14}N_2$ (Figure 1a). Each dimer is connected to six different pyridine-2,3-dicarboxylate moieties and each pyridine-2,3-dicarboxylate is connected to three different dimers, thus giving rise to a two-dimensional layer with 3^6 topology (Figure 1b). The two-dimensional layers are connected by the terephthalate units that complete the three-dimensional structure (Figure 2). The presence of coordinated water molecules and the spatial displacement of the pyridine-2,3-dicarboxylate units give rise to two distinct pockets, hydrophilic and hydrophobic, respectively (Figure 3a). Additionally, the presence of two coordinated water molecules [O(5) and O(6)] in close proximity gives rise to O–H···O hydrogen bonds. These interactions also result in a one-dimensional helical arrangement (Figure 3b), which may be due to the presence of a 2_1 axis in the structure. In addition, the coordinated water molecules also interact with other carboxylate oxygen atoms with O···O contact distances in the range 2.761(3)–2.855(4) Å and O–H···O angles in the range 156–176°. The observed hydrogen-bond interactions are listed in Table 2. The two-dimensional layer with 3^6 topology appears to be unique and has been observed for the first time in a highly coordinated lanthanide carboxylate.

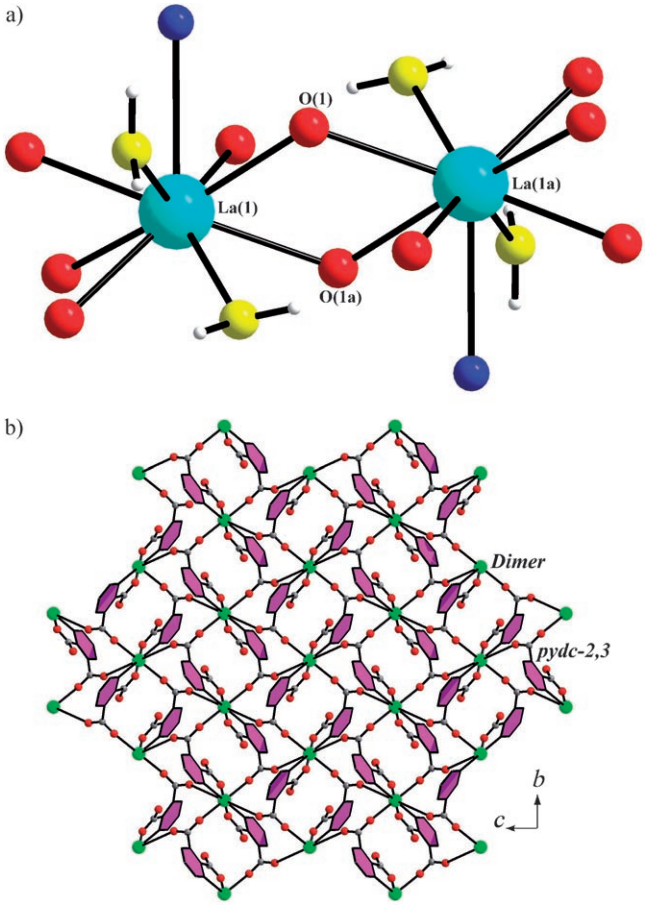

Figure 1. a) The dimer, $La_2O_{14}N_2$, formed by the connectivity between LaO_8N polyhedra through two μ_3 oxygen atoms [O(1)] in **I**. b) Two-dimensional layer in the *bc* plane formed by the connectivity between the $La_2O_{14}N_2$ dimers and the pyridine-2,3-dicarboxylate (pydc-2,3) units. The dimers are represented as a single sphere for simplicity.

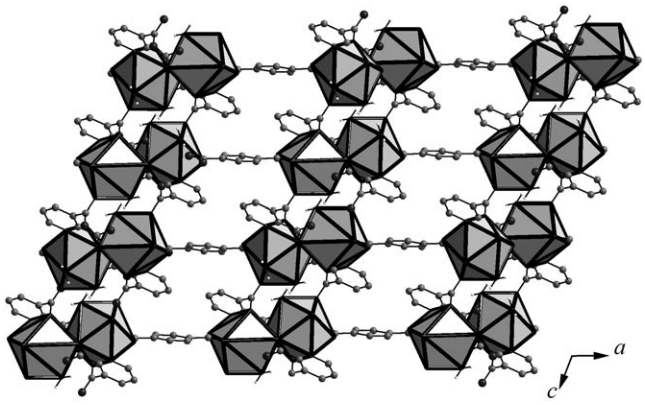

Figure 2. Three-dimensional structure formed by the connectivity between the two-dimensional layers and the benzene-1,4-dicarboxylate units.

Well-known examples for the observation of 3^6 topology are the $CdCl_2$ structure and in UO_2^{2+}-type coordinated structures (where all six ligands are in the equatorial plane).[10] To compare the present two-dimensional connectivity between La^{3+} ions and quinolinate anions with that of $CdCl_2$ and UO_2^{2+}-type coordinated structures, we represented the dimer and the quinolinate units as spheres arranged in a two-dimensional lattice (Figure 4a). It then immediately becomes evident that the present structure has a close similarity to the $CdCl_2$ structure (Figure 4b). The UO_2^{2+}-type coordinated structure, though it appears to be comparable, has the ligand connecting only two metal centers (Figure 4c), whereas in $CdCl_2$ the ligands (Cl^-) connect with three metal centers. In the present structure, each dimer is connected to six quinolinate anions and each quinolinate anion is connected to three different dimers, which is akin to the situation found in the $CdCl_2$ structure. In addition, the topological arrangement of the different layers in the present structure also mimics the arrangement of the layers found in the $CdCl_2$ structure (Figure 5a and b).

Thermal studies: Thermogravimetric analysis (TGA) was carried out in air (flow rate 20 mL min^{-1}) in the temperature range 30–850 °C (heating rate 5 °C min^{-1}; see Figure S2 in the Supporting Information). The results indicate that compounds **I–III** all behave in a similar fashion. An initial weight loss (≈8%) in the temperature range 170–220 °C for all three compounds may be due to the loss of coordinated water molecules, and the second weight loss, which occurs in

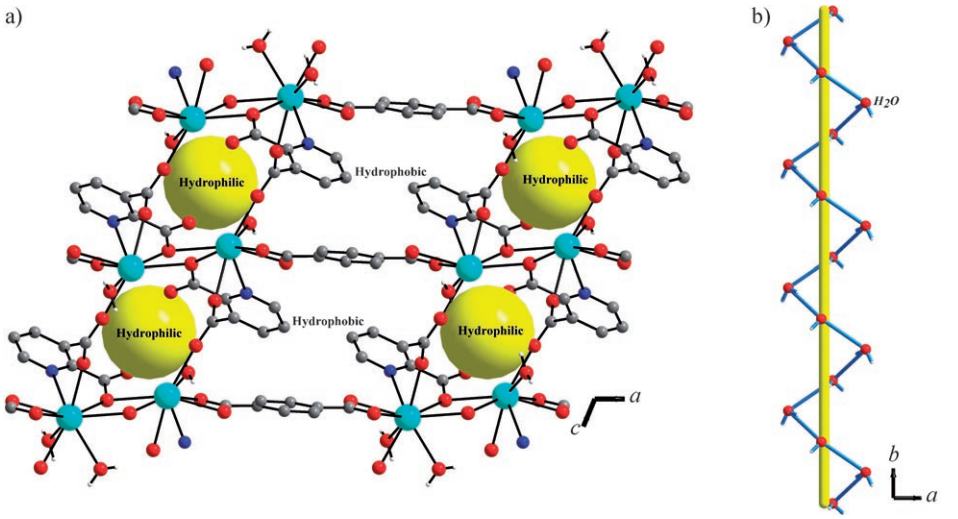

Figure 3. a) Hydrophilic and hydrophobic cavities within the three-dimensional structure. b) Arrangement of the coordinated water molecules to form helical one-dimensional chains (see text).

Table 2. Important hydrogen-bond interactions in $[La_2(H_2O)_4][\{C_5H_3N(COO)_2\}_2\{C_6H_4(COO)_2\}]$ (**I**).

D–H···A[a]	D–H [Å]	H···A [Å]	D···A [Å]	D–H···A [°]
O(5)–H(5A)···O(7)#1	0.94	1.82	2.761(3)	175.9
O(5)–H(5B)···O(6)#2	0.94	2.18	3.039(3)	151
O(6)–H(6A)···O(8)#3	0.94	1.83	2.769(4)	175
O(6)–H(6B)···O(3)#4	0.94	1.97	2.855(4)	156

[a] #1: x, $1+y$, z; #2: $1-x$, $1/2+y$, $3/2-z$; #3: x, $3/2-y$, $1/2+z$; #4: $1-x$, $2-y$, $1-z$.

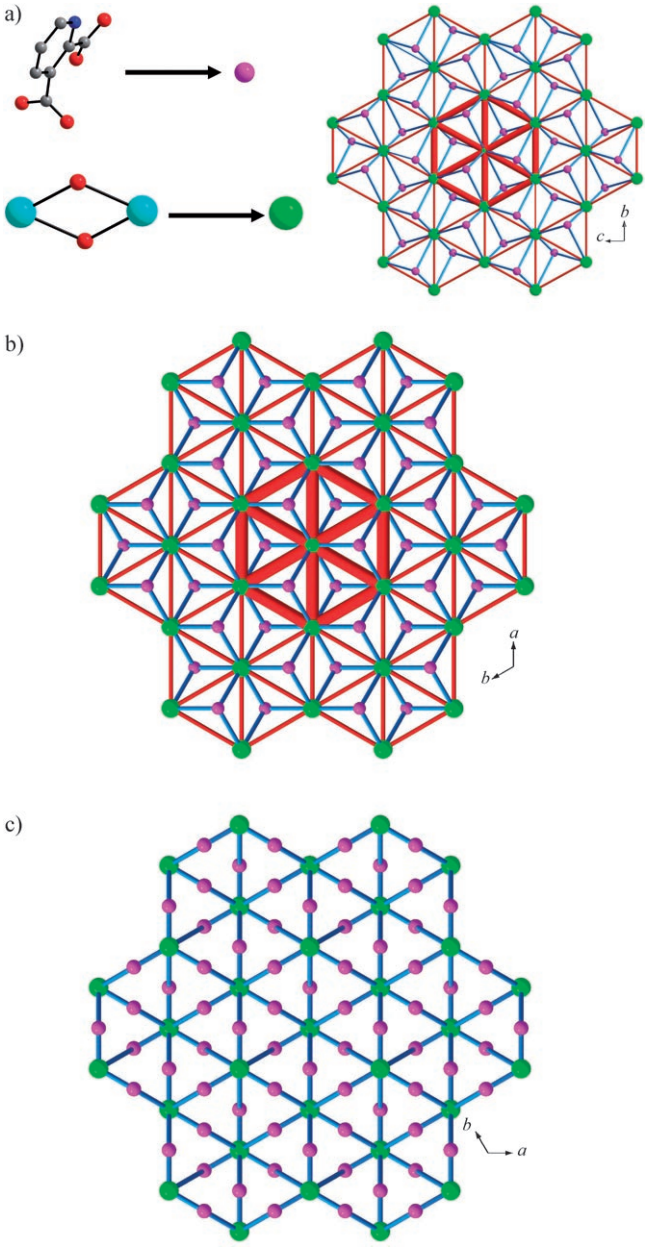

Figure 4. a) Connectivity between the six connected dimeric units (green spheres) and the three connected pyridine-2,3-dicarboxylate moieties (purple spheres) forming the 3^6 topology (see text). b) Structure of $CdCl_2$. Cd atoms: green; Cl atoms: purple. Note the close structural similarity between the two-dimensional layer of **I** and $CdCl_2$. c) UO_2^{2+}-type coordinated structure with 3^6 topology. Metal atoms: green; ligands: purple. Note the differences in the connectivity of this structure and **I**.

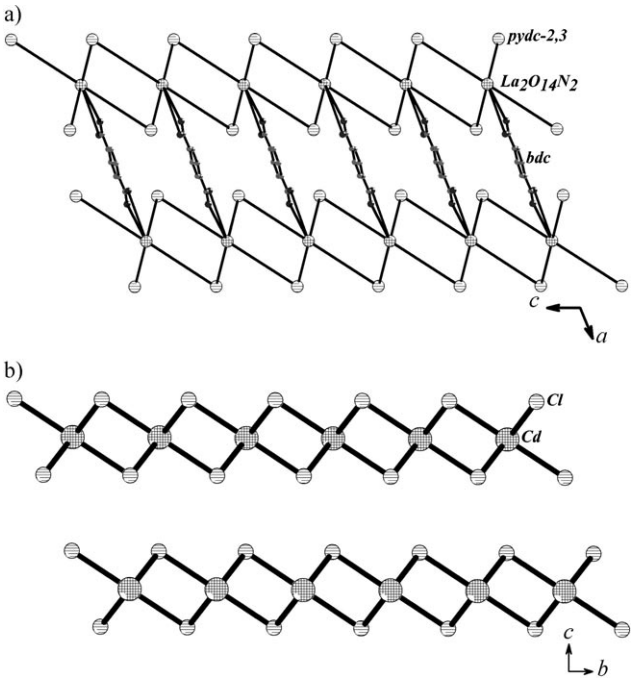

Figure 5. a) Three-dimensional connectivity of the layers in **I** through benzene-1,4-dicaboxylate moieties. b) Arrangement of layers in the $CdCl_2$ structure. Note the similarity in the arrangement of layers in the structures.

two steps in the temperature range 280–480 °C, corresponds to the loss of all the carboxylate moieties. The total observed weight loss corresponds well with the loss of the carboxylate and water molecules: 64 (calcd 61.4), 62 (calcd 59.9), and 63 % (calcd 60.64 %) for **I**–**III**, respectively. The final calcined product was found to be crystalline by powder XRD and corresponds to La_2O_3 (JCPDS: 00-002-0688), Pr_6O_{11} (JCPDS: 00-042-1121), and Nd_2O_3 (JCPDS: 00-021-0579 and 00-006-0408), respectively. The three compounds in the present study are isostructural, and therefore to investigate the physical properties we chose to study the lanthanum-containing compound, $[La_2(H_2O)_4][\{C_5H_3N(COO)_2\}_2\{C_6H_4(COO)_2\}]$ (**I**).

The TGA studies clearly revealed a single-step weight loss in the range 170–220 °C, which corresponded with the possible loss of the coordinated water. To probe the reversibility of water adsorption, we employed ex situ powder XRD studies. For this purpose, the La-containing sample was heated at three different temperatures (180, 200, 220 °C) and the powder XRD patterns were compared with that of **I** (Figure 6 A). The sample heated at 220 °C indicated the disappearance of some of the peaks at high 2θ values (>13) although the main peak at around 6.7° appears to remain unchanged, but with reduced intensity. In addition, some broadness in the peak width can also be noticed, which suggests that the loss of the coordinated water at 220 °C may lead to the loss of crystallinity. The dehydrated sample (heated at 220 °C) was kept in the open air (laboratory conditions) and the powder XRD patterns were recorded periodically as a function of time (Figure 6 B). As can be

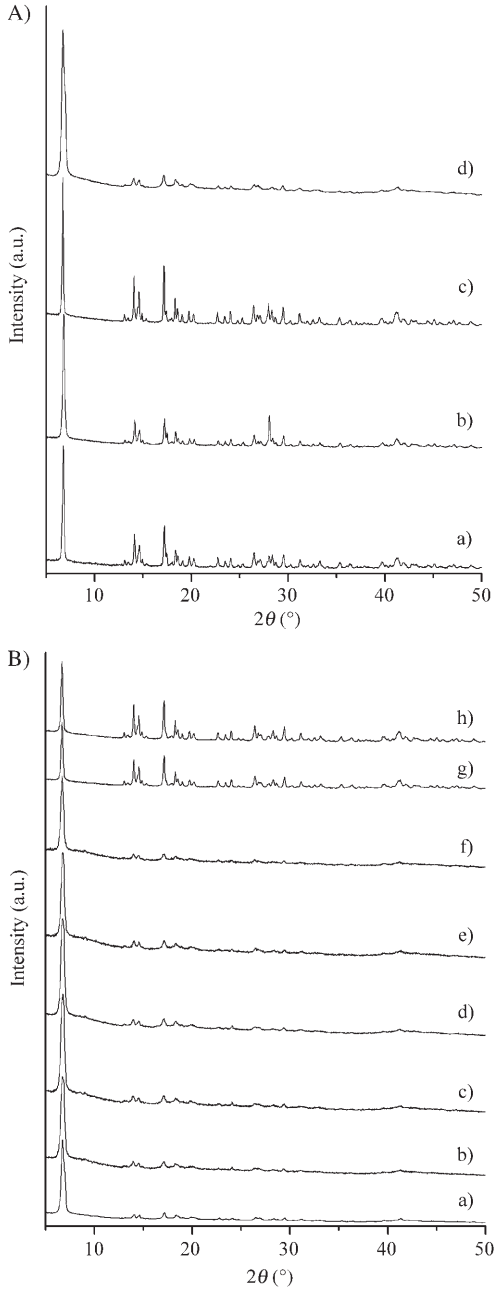

Figure 6. A) Ex situ powder XRD study of $[La_2(H_2O)_4][\{C_5H_3N(COO)_2\}_2\text{-}\{C_6H_4(COO)_2\}]$ (**I**): a) RT; b) 180; c) 200; d) 220 °C. Note the change in the XRD pattern at 220 °C. B) Ex situ XRD plots of the dehydrated sample of **I** as a function of time: a) fully dehydrated; b) 1 h; c) 10 h; d) 1 day; e) 2 days; f) 7 days; g) fully rehydrated. h) fully deuterated sample (see text).

noted, the samples appear to remain dehydrated for at least one week, which indicates the stable nature of the dehydrated state. The dehydrated sample, when heated with water at 75 °C for 12 h in an autoclave, immediately returns to the original hydrated phase.

To understand this possible reversible hydration behavior of **I**, we carried out in situ diffuse reflectance Fourier transform IR spectroscopic (DRIFTS) studies (Perkin–Elmer, Spectrum 2000, mercury cadmium telluride detector) in the range from 25 to 250 °C. The coordinated water band at 3535 cm^{-1} was monitored as a function of temperature and the results are presented in Figure 7a. As can be noted, the

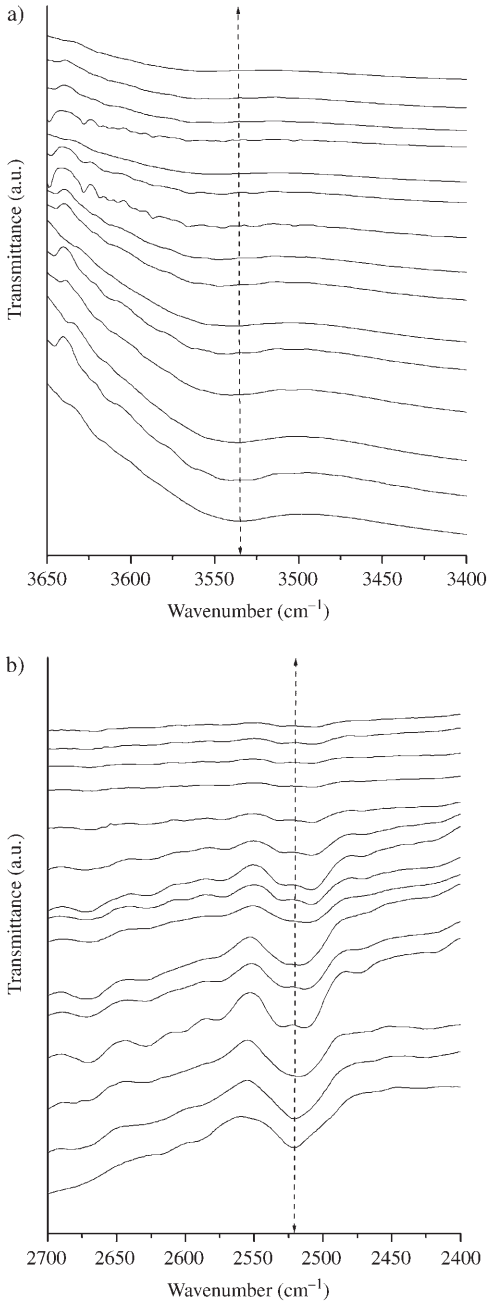

Figure 7. In situ DRIFTS of **I** as a function of temperature showing the disappearance of the bands a) H_2O, 3535 cm^{-1}, and b) D_2O, 2520 cm^{-1}. The dashed line is a guide to the eye.

band gradually disappears with increasing temperature, thus confirming the removal of the coordinated water molecules from the structure. To investigate the reversible uptake of H_2O, we made efforts to replace the coordinated water with D_2O and study the dehydration behavior. For this, the fully

dehydrated sample was heated in a similar fashion with D_2O in an autoclave, and the deuterated sample studied by using DRIFTS. The IR spectra of the deuterated sample show a peak around 2520 cm^{-1}, which corresponds to the D_2O stretching vibration.[17] The D_2O-exchanged sample does not exhibit the peak corresponding to water at 3535 cm^{-1}, which suggests that the coordinated water molecules were completely replaced by D_2O. The DRIFTS studies of the deuterated sample also exhibited a behavior similar to that of the as-prepared sample when heated under identical conditions. Thus, the peak at 2520 cm^{-1} also loses intensity with increasing temperature (Figure 7b). This study clearly establishes the complete reversibility of the hydration in **I**.

Luminescence studies: Lanthanide ions, generally, have low molar absorptivity, which results in weak emission when excited directly. Significant emission, characteristic of the lanthanide ion, however, can be observed by employing suitable chelates that can absorb and transfer the energy to the lanthanide ion.[18] In most cases, the direct excitation of the ligand leads to a singlet state, which goes to a triplet state via an intersystem crossing. The emission from the metal is observed when a nonradiative energy transfer occurs from the triplet state of the ligand to the lanthanide ion.[19] The lanthanide ion can then emit a photon or relax through a series of nonradiative processes. This phenomenon is known as the "antenna effect".[19b,20] It has been shown that the lanthanide-centered emission can be sensitized by molecules with π electrons. The success of the transfer of energy is reflected in the suppression of the intra-ligand emission. It has been shown that the nitrogen-containing ligands, which directly bond with the lanthanide ion, are more efficient in transferring the energy, which results in stronger emission.[21] Presently, we have both the nitrogen-containing ligands (pyridine) and the regular conjugated π systems (benzene) that bind with the lanthanide. Both can absorb strongly in the UV region and sensitize the lanthanide ion through the antenna effect described above. The high-intensity band at around 300 nm in the UV/Vis spectra of these compounds indicates the intra-ligand energy-transfer process due to the $\pi\rightarrow\pi^*$ or $n\rightarrow\pi^*$ transitions (see Figures S3 and S4 in the Supporting Information).

In the emission spectra of the sodium salts of the two dicarboxylates, the benzene-1,4-dicarboxylate salt shows a broad emission centered around 365 nm, whereas the pyridine-2,3-dicarboxylate salt shows a broad emission at 380 nm, along with two low-intensity peaks at 420 and 488 nm, when excited by a wavelength (λ_{ex}) of 300 nm (see Figure S5 in the Supporting Information). The emission peaks arise from the $\pi^*\rightarrow n$ and $\pi^*\rightarrow\pi$ transitions of the two aromatic dicarboxylates. Compounds **I**–**III** also exhibit four emission bands centered at 356, 380, 420, and 488 nm ($\lambda_{ex}=$ 300 nm). This result clearly indicates that the emissions in the present compounds are due to the intra-ligand energy transfer, which has been observed in many lanthanide carboxylate systems.[22] It is believed that the benzene carboxylate ligands act as a sensitizer for the lanthanide ions.

To investigate the luminescence from the metal-centered emission in the present compounds, we partially doped Eu (2 mol%, **Ia**, and 4 mol%, **Ib**) and Tb (2 mol%, **Ic**, and 4 mol%, **Id**) in place of La in **I**. The concentrations of Eu in **Ia** and **Ib** as well as of Tb in **Ic** and **Id** were based on the notional composition in the initial mixture (see Experimental Section). The success of the energy transfer from the aromatic π system to the metal ion is clearly indicated by the suppression of the intra-ligand emission in the luminescence spectra along with the observation of the characteristic colors of the doped ion under UV illumination (red/pink (Eu^{3+}) and green (Tb^{3+}), see Figure S6 in the Supporting Information).

The solid-state photoluminescence spectra of **I** and **Ia–d** are presented in Figure 8a and b. As can be noted, the main intra-ligand emission band is suppressed in the doped samples (**Ia**–**d**) followed by the observation of the emission lines characteristic of the metal. It is known that Eu^{3+} ions can emit $^5D_0$ (red), $^5D_1$ (green), and $^5D_2$ (blue) regions, the emissions being dependent on the host lattice.[19b] The emissions from the Tb^{3+} ions are mainly from the $^5D_4$ (green) region, and in some cases $^5D_3$ (blue) emissions have also been observed.[19b] In the present compounds, we observed $^5D_0\rightarrow{}^7F_J$ ($J=0$–4) and $^5D_1\rightarrow{}^7F_J$ ($J=1$, 2) emission bands for Eu^{3+} ions and $^5D_4\rightarrow{}^7F_J$ ($J=3$–6) emission bands for the Tb^{3+} ions, when excited by a wavelength of 300 nm. For **Ia** and **Ib**, the emission bands at 530–540 and 556 nm correspond to $^5D_1\rightarrow{}^7F_1$ and $^5D_1\rightarrow{}^7F_2$ transitions, respectively. The bands at 578, 590–596, 615, 650, and 693 nm correspond to $^5D_0\rightarrow{}^7F_0$, $^5D_0\rightarrow{}^7F_1$, $^5D_0\rightarrow{}^7F_2$, $^5D_0\rightarrow{}^7F_3$, and $^5D_0\rightarrow{}^7F_4$ transitions, respectively (Figure 8a). Observation of the transition from the $^5D_1$ state to the ^7F_J state of Eu^{3+} in **Ia** and **Ib** is noteworthy, as most of the Eu-containing compounds show transitions only from the $^5D_0$ state to the ^7F_J state in the visible region (400–800 nm).[23] The 4% Eu-doped sample (**Ib**) shows less intra-ligand emission than the 2% Eu-doped sample (**Ia**), which indicates that the higher dopant level at the lanthanum site facilitates the transfer of more energy from the aromatic ligands. This observed behavior may not be expected to be linear for higher concentrations of Eu^{3+}, as the metal-centered emission would begin to undergo self-quenching.[21]

It has been observed that the lanthanide emissions are sensitive to the local environment around the lanthanide ion.[19b] The subtle differences in the emission behavior has been rationalized by invoking the symmetry of the coordination geometry around the lanthanide ions.[24] In the present compounds, it is notable that the $^5D_0\rightarrow{}^7F_2$ transition has a much larger intensity than the $^5D_0\rightarrow{}^7F_1$ transition. This has been employed to prove the coordination state and the site symmetry around the Eu^{3+} ion, since the $^5D_0\rightarrow{}^7F_1$ emission is due to the magnetic dipole and independent of the ligand environment.[23b] The $^5D_0\rightarrow{}^7F_2$ emission, on the other hand, is due to the electric dipole and is sensitive to the crystal field symmetry.[24b] In **Ia** (2% Eu) and **Ib** (4% Eu), the intensity ratios of the $^5D_0\rightarrow{}^7F_2$ and $^5D_0\rightarrow{}^7F_1$ transitions are 5.2 and 3.92, respectively. The sensitive dependence of the

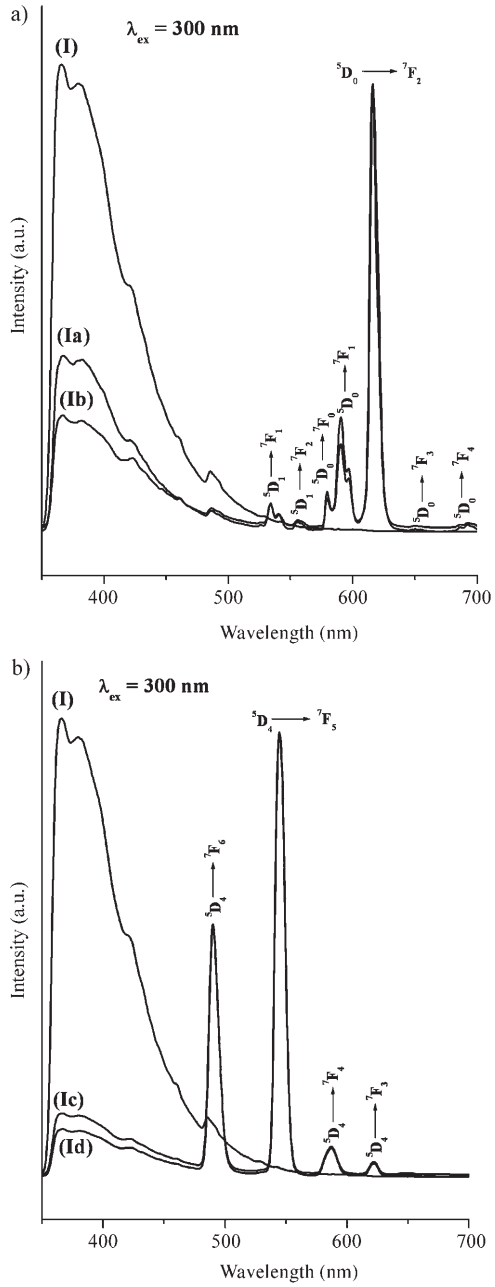

Figure 8. Room-temperature photoluminescence spectra of a) **I** and the corresponding Eu-doped compounds **Ia** (2 mol% Eu) and **Ib** (4 mol% Eu); b) **I** and the corresponding Tb-doped compounds **Ic** (2 mol% Tb) and **Id** (4 mol% Tb).

emission on the coordination can be explored further in the present compounds as it has been established that the coordinated water molecules can be reversibly adsorbed. Therefore, the dehydrated samples can provide further insights into the local symmetry of the La^{3+} ions, especially in the Eu^{3+}-doped compounds in luminescence studies. Since the dehydrated samples appear to be stable under atmospheric conditions, we carried out photoluminescence studies on the dehydrated samples (see Figure S7 in the Supporting Information). The studies indicate a similar ligand-sensitized metal-centered emission with characteristic lines (see Figure S7 in the Supporting Information). The intensity ratios of the $^5D_0 \rightarrow {}^7F_2$ and $^5D_0 \rightarrow {}^7F_1$ transitions are 4.2 and 3.6, respectively, for the 2% Eu and 4% Eu samples. The reduced values of the ratio in the dehydrated sample indicate that the lanthanide ions have less coordination and are also more symmetric. The fully hydrated sample contains two water molecules positioned adjacent to each other (*cis–cis* arrangement) in one face of the trigonal prism, as part of the nine coordination of the La^{3+} ion (see Figure S8 in the Supporting Information), and can exert some strain. It is also known that the *cis* structure is generally less symmetric. During dehydration, the bound water molecules are removed, which would give rise to a seven-coordinated La^{3+} ion that is probably much less strained than the nine-coordinated La^{3+} site.

For the Tb^{3+}-doped compounds (**Ic** and **Id**), the emission bands at 490, 543, 587, and 622 nm can be assigned to the $^5D_4 \rightarrow {}^7F_6$, $^5D_4 \rightarrow {}^7F_5$, $^5D_4 \rightarrow {}^7F_4$, and $^5D_4 \rightarrow {}^7F_3$ transitions, respectively, when excited by a 300 nm source. Again, the higher concentration of Tb^{3+} ions in **Id** shows considerably more quenching of the intra-ligand transition (Figure 8b). The present results are qualitative, and the emission observed in these compounds could be compared to the emissions for other similar compounds.[21]

Lifetime studies: To study the luminescence lifetime of the excited states, we used the 4%-doped samples (**Ib** = Eu; **Id** = Tb). The 615 nm emission ($^5D_0 \rightarrow {}^7F_2$) for the Eu^{3+} sample and the 543 nm emission ($^5D_4 \rightarrow {}^7F_5$) for the Tb^{3+} sample were monitored with lifetime studies by employing 300 nm excitation at room temperature (Figure 9). The luminescence decay behavior can be fitted into a single-exponential function [Eq. (1)], in which I and I_0 are the luminescence intensities at times t and 0 and τ is defined as the luminescence lifetime.

$$I = I_0 \exp(-t/\tau) \quad (1)$$

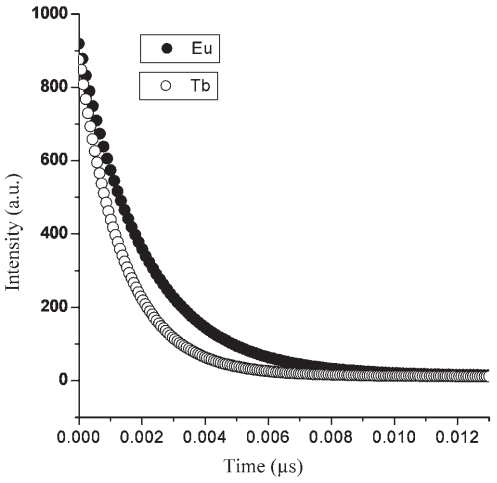

Figure 9. Room-temperature luminescence decay curves for compounds **Ib** (4% Eu) and **Id** (4% Tb).

The studies indicate lifetime values of 29.4 μs for the 4% Eu^{3+}-doped sample and 14.3 μs for the 4% Tb^{3+}-doped sample. The luminescence lifetime values for the doped samples in the present study appear to be smaller than those obtained generally for the pure Eu^{3+} and Tb^{3+} carboxylates reported in the literature.[24b,25]

Up-conversion studies: Up-conversion phosphors, capable of converting long-wavelength radiation into a shorter wavelength through multiphoton processes, have attracted much attention.[26] Generally, trivalent lanthanides are suitable for such an up-conversion process due to the availability of a number of electronic states, including many intermediate levels.[19b] Up-conversion studies have been carried out on inorganic rare-earth materials (oxides, silicates, fluorides, etc.),[27] and such investigations are beginning to emerge in rare-earth-based MOF compounds as well.[25] Among the present compounds, the Pr- and Nd-containing materials (**II** and **III**) may be attractive for the study of up-conversion behavior. The UV/Vis spectrum of compound **III** is shown in Figure 10a. As can be noted, the sample exhibits intra-ligand $\pi\rightarrow\pi^*$ or $n\rightarrow\pi^*$ transitions of the aromatic ligands at lower wavelengths (<330 nm). In addition, the absorption bands in the range 330–900 nm show detailed Stark splitting of the eigenstates by the crystal field effect.[28] The details of the Stark components, however, could not be resolved clearly from the absorption spectrum due to the overlap of the excited upper Stark levels of the ground state, which results in a complex absorption spectrum. The UV/Vis spectra of compound **II** also show some Stark splitting (see Figure S3 in the Supporting Information).

A schematic of the various energy-transfer processes in the up-conversion emission with Nd^{3+} ions is shown in Figure 10b. We employed the energy corresponding to the absorption band, $^4I_{9/2}\rightarrow{}^4G_{5/2}$ (580 nm), as the excitation energy for examining the up-conversion behavior in **III** (Figure 10a). This energy level is far from the intra-ligand absorption bands. The luminescence of **III** at short wavelengths is expected to result from the $^4D_{3/2}$ levels, and the direct excitation to either the $^4D_{3/2}$ or $^4D_{5/2}$ level is limited as they are close to the intra-ligand absorption bands. The excitation wavelength ($\lambda\approx580$ nm) was tuned to optimize the up-conversion excitation efficiency of populating the $^4F_{3/2}$ levels and efficient re-excitation from the $^4F_{3/2}$ to the $^4D_{5/2}$ level. The possible up-conversion excitation pathways (dashed lines) and corresponding transitions (solid lines) for the luminescence of Nd^{3+} ions are summarized in Figure 10b. The ground-state absorption (GSA) is responsible for the excitation from the $^4I_{9/2}$ level to the $^4G_{5/2}$ level. The excited $^4G_{5/2}$ levels relax nonradiatively to the $^4F_{3/2}$ levels, where some populations take part in excited-state absorption (ESA) and the remainder relax to lower energy levels. Another excitation from the $^4F_{3/2}$ level populates the excited $^4D_{5/2}$ levels from the ESA that also relax nonradiatively to the $^4D_{3/2}$ levels from which up-converted luminescence is emitted. Figure 10c shows the up-converted luminescence spectrum from the $^4D_{3/2}$ levels for the 580 nm excitation.

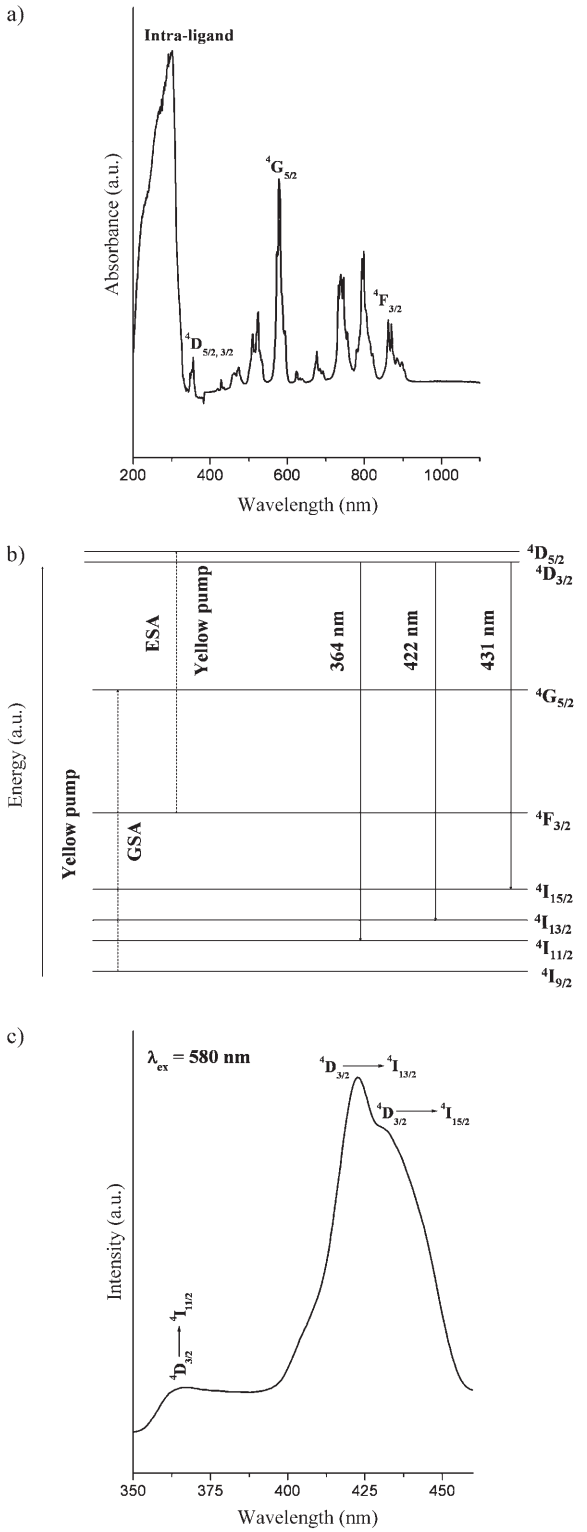

Figure 10. a) Room-temperature UV/Vis absorption spectrum of **III**. b) Energy-level diagram for the Nd^{3+} ion in **III**. The dotted and solid lines indicate yellow pumping (580 nm) and the transitions related to the observed emissions, respectively. c) Up-converted luminescence spectrum of **III** at room temperature excited by using radiation at $\lambda_{ex}=580$ nm.

The emission spectrum has a peak at 422 nm and two shoulders at 364 and 431 nm, which correspond to the $^4D_{3/2} \rightarrow {}^4I_{13/2}$, $^4D_{3/2} \rightarrow {}^4I_{11/2}$, and $^4D_{3/2} \rightarrow {}^4I_{15/2}$ transitions, respectively. Similar emission is also observed for the dehydrated sample, which indicates that the up-conversion process is element specific and not dependent on the coordination environment around the element (see Figure S8 in the Supporting Information).

The correlation between the excitation intensity and that of the up-converted luminescence intensity can be examined by carrying out further studies. Thus, a series of sterile glass plates were placed sequentially in the pathway between the excitation source and the sample. The decrease in the excitation intensity per glass plate was determined by UV/Vis spectroscopy in the transmission mode and normalized with respect to the transmission obtained in the absence of any glass slides. The normalized transmission intensities (I_{ex}) as a function of the number of glass plates, along with the emission intensities (I_{em}), are shown in Figure 11 A. This study can also give some indications of the number of photons involved in the up-conversion process. Accordingly, if n is the number of photons absorbed, then [Eqs. (2)–(4)]

$$I_{em} \propto (I_{ex})^n \quad (2)$$

$$\text{or } I_{em} = A(I_{ex})^n \quad (3)$$

$$\text{or } \log I_{em} = A\,1 + n\log I_{ex} \quad (4)$$

The value of n can be obtained from the log–log plot of I_{em} versus I_{ex} (I_{em} = emission intensity of any luminescence peak, I_{ex} = intensity of the excitation energy, and n = number of photons responsible for the emission process). The log–log plot for the emissions at 422, 431, and 364 nm, which correspond to $^4D_{3/2} \rightarrow {}^4I_{13/2}$, $^4D_{3/2} \rightarrow {}^4I_{15/2}$, and $^4D_{3/2} \rightarrow {}^4I_{11/2}$, respectively, are shown in Figure 11 B. A fit of the lines gave a value for n close to 2 (the value of the slope), thus indicating that all three emissions are based on two-photon absorption. Similar values for the slopes have been obtained before for the two-photon up-conversion processes in Nd^{3+} compounds.[27]

The Pr^{3+} compound (**II**), when subjected to an identical study, did not show any up-conversion behavior. A blue up-conversion through a two-photon absorption ($^3H_4 \rightarrow {}^1G_4$ and $^1G_4 \rightarrow {}^3P_0$) has been observed in many Pr^{3+}-containing compounds when excited by IR radiation.[27] Such a process was not possible in our present investigation because we employed visible light as the excitation source, which resulted in the nonobservation of the up-conversion processes in **II**.

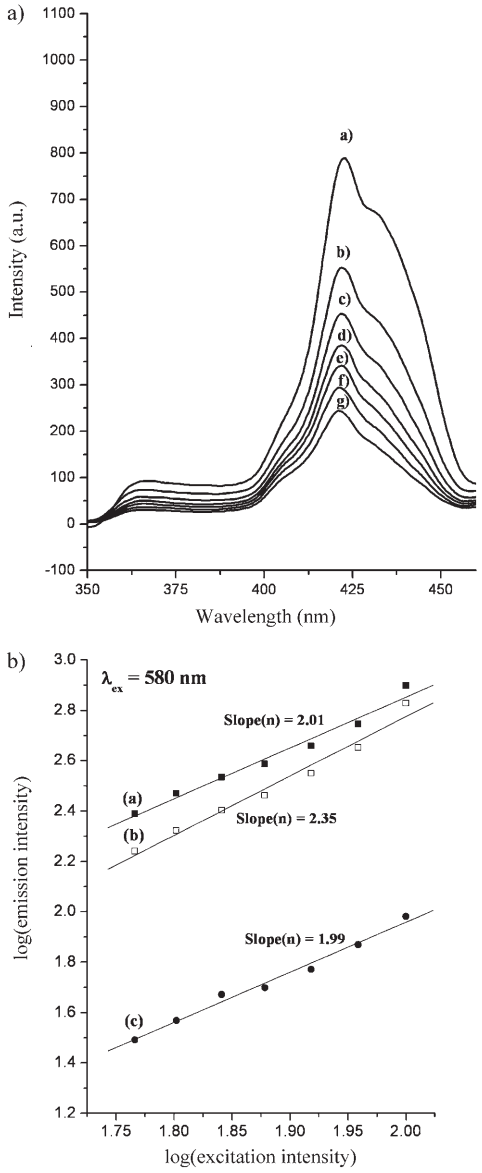

Figure 11. A) Dependence of the observed emission on the excitation intensity of **III.** a) 100; b) 90.94; c) 82.84; d) 75.55; e) 69.34; f) 63.4; g) 58.37 %. B) Log–log plot of the dependence of excitation intensity on the emission intensity at different up-converted emissions: λ = 422 (a), 431 (b), and 364 nm (c).

Conclusion

The synthesis, structure, and photophysical properties of a new series of lanthanide mixed carboxylate systems have been accomplished. The formation of $CdCl_2$-related layers with 3^6 topology is interesting and has been observed for the first time in a lanthanide carboxylate system. The observation of metal-centered emission in samples doped with Eu^{3+} (red/pink) and Tb^{3+} (green), and a blue luminescence in a Nd^{3+} sample (**III**) through an up-conversion process, is noteworthy. The coordinated water molecules can be reversibly adsorbed and appear to have some effect on the photophysical behavior of the prepared compounds.

Experimental Section

Synthesis and initial characterization: All the compounds were prepared by employing the hydrothermal method. In a typical synthesis, for **I**, La-

$(NO_3)_3$ (0.163 g, 0.5 mM) was dispersed in water (2 mL). Pyridine-2,3-dicarboxylic acid (0.085 g, 0.5 mM), benzene-1,4-dicarboxylic acid (0.083 g, 0.5 mM), and piperazine (0.086 g, 1 mM) were added under continuous stirring. The mixture was homogenized for 30 min at room temperature. The final mixture was then sealed in a 7 mL PTFE-lined autoclave and heated at 125 °C for three days under autogenous pressure. The initial pH of the reaction mixture was 4, and no appreciable change in pH was noted after the reaction. The final product, which contained colorless block-type crystals along with white powder, was filtered, washed with deionized water under vacuum, and dried under ambient conditions (yield ≈70 % based on La). The white powder obtained along with the single crystals was found to be of the same phase as the single crystals by powder XRD studies. For the preparation of isostructural Pr (**II**) and Nd (**III**) compounds, $Pr(NO_3)_3$ (0.164 g, 0.5 mM) and $Nd(NO_3)_3$ (0.165 g, 0.5 mM) were used in place of $La(NO_3)_3$ and the composition and reaction conditions were kept identical to those in the synthesis of **I**. In both the cases, the resulting product contained large quantities of pale green (Pr) and pale violet (Nd) polycrystalline powder with similar yields. The compounds with Eu (2 mol %, **Ia**; 4 mol %, **Ib**) and Tb (2 mol %, **Ic**; 4 mol %, **Id**) substituted in place of La (**I**) were also prepared by employing similar synthesis procedures, which resulted in fine, uniform powder samples with high yields. Elemental analysis calcd (%) for **I**: C 31.27, H 2.13, N 3.32; found: C 31.01, H 2.17, N 3.19; calcd for **II**: C 31.24, H 2.12, N 3.30; found: C 31.11, H 2.16, N 3.26; calcd for **III**: C 30.88, H 2.10, N 3.28; found: C 30.61, H 2.07, N 3.21; calcd for **Ia**: C 31.25, H 2.13, N 3.31; found: C 31.17, H 2.09, N 3.35; calcd for **Ib**: C 31.23, H 2.13, N 3.31; found: C 31.15, H 2.15, N 3.24; calcd for **Ic**: C 31.24, H 2.13, N 3.31; found: C 31.17, H 2.12, N 3.37; calcd for **Id**: C 31.21, H 2.13, N 3.31; found: C 31.07, H 2.08, N 3.20. Energy-dispersive X-ray analysis of the powder sample indicated the presence of both La and Eu (**Ia** and **Ib**) and La and Tb (**Ic** and **Id**; see Figures S9 and S10 in the Supporting Information)

Powder XRD patterns were recorded in the 2θ range of 5–50° by using $Cu_{K\alpha}$ radiation (Philips X'pert; Figure 12). The XRD pattern for the La compound (**I**) indicated that the product was new; the patterns were entirely consistent with the simulated XRD pattern generated based on the structures determined using the single-crystal XRD. The Pr (**II**)- and Nd (**III**)-containing samples as well as the doped ones are highly crystalline and have XRD patterns comparable to that obtained for the La (**I**) compound (Figure 12). IR spectra for all the compounds were recorded as KBr pellets (Perkin–Elmer, Spectrum 1000). The observed IR frequencies for compounds **I–III** are listed in Table 3 (see Figure S11 in the Supporting Information).

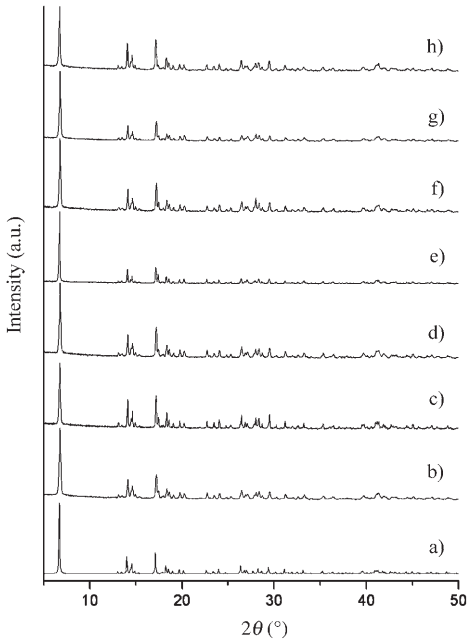

Figure 12. Powder XRD patterns of the prepared compounds. a) simulated from the single-crystal structure of **I**. Experimental results of: b) **I**; c) **II**; d) **III**; e) **Ia**; f) **Ib**; g) **Ic**; h) **Id**. Note that all the XRD patterns are identical, which indicates the phase purity of the as-prepared samples.

Table 3. Observed IR bands for $[La_2(H_2O)_4][\{C_5H_3N(COO)_2\}_2\{C_6H_4(COO)_2\}]$ (**I**), $[Pr_2(H_2O)_4][\{C_5H_3N(COO)_2\}_2\{C_6H_4(COO)_2\}]$ (**II**), and $[Nd_2(H_2O)_4][\{C_5H_3N(COO)_2\}_2\{C_6H_4(COO)_2\}]$ (**III**).

Bands	**I** [cm^{-1}]	**II** [cm^{-1}]	**III** [cm^{-1}]
ν_{as}(O–H)	3535 (m)	3540 (m)	3537 (m)
ν_{s}(O–H)	3357(s)	3346 (s)	3346 (s)
ν_{s}(C–H)$_{aromatic}$	3064 (w)	3053 (w)	3050 (w)
$\delta(H_2O)$	1620 (m)	1615 (m)	1618 (m)
ν_{as}(COO)	1578 (s)	1568 (s)	1570 (s)
ν_{s}(COO)	1397 (s)	1397 (s)	1390 (s)
$\delta(CH_{aromatic})_{in\text{-}plane}$	1105 (m)	1093 (m)	1102 (m)
$\delta(CH_{aromatic})_{out\text{-}of\text{-}plane}$	834 (m)	837 (m)	845 (m)
δ(COO)	755 (m)	757 (m)	755 (m)

Single-crystal structure determination: A suitable single crystal of **I** was carefully selected under a polarizing microscope and glued to a thin glass fiber. The single-crystal data were collected on a Bruker AXS smart Apex CCD diffractometer at 293(2) K. The X-ray generator was operated at 50 kV and 35 mA using $Mo_{K\alpha}$ ($\lambda = 0.71073$ Å) radiation. Data were collected with an ω scan width of 0.3°. A total of 606 frames were collected in three different settings of ϕ (0, 90, 180°) while keeping the sample-to-detector distance fixed at 6.03 cm and the detector position (2θ) fixed at −25°. The data were reduced using SAINTPLUS,[29] and an empirical absorption correction was applied using the SADABS program.[30] The structure was solved and refined using SHELXL97,[31] which is present in the WinGx suite of programs (Version 1.63.04a).[32] All the hydrogen atoms of the carboxylic acids and the bound water molecules were initially located in the difference Fourier maps, and for the final refinement the hydrogen atoms were placed in geometrically ideal positions and refined in the riding mode. Restraints for the bond lengths were used during the refinement for keeping the hydrogen atoms of the water molecules. Final refinement included atomic positions for all the

Table 4. Crystal data and structure refinement parameters for $[La_2(H_2O)_4][\{C_5H_3N(COO)_2\}_2\{C_6H_4(COO)_2\}]$ (**I**).

empirical formula	$C_{22}H_{18}N_2O_{16}La_2$
formula weight	844.20
crystal system	monoclinic
space group	$P2_1/c$ (no.14)
a [Å]	14.280(3)
b [Å]	6.9480(14)
c [Å]	13.662(3)
α[°]	90.0
β [°]	112.380(3)
γ [°]	90.0
volume [$Å^3$]	1253.4(4)
Z	2
T [K]	293(2)
ρ_{calcd} [$g\,cm^{-3}$]	2.237
μ [mm^{-1}]	3.450
θ range [°]	1.54 to 27.99
λ ($Mo_{K\alpha}$) [Å]	0.71073
R indices [$I > 2\sigma(I)$]	R_1=0.0202, wR_2=0.0557[a]
R indices (all data)	R_1=0.0238, wR_2=0.0697[a]

[a] $R_1 = \Sigma \| F_0| - |F_c \| / \Sigma |F_0|$; $wR_2 = \{\Sigma[w(F_0^2 - F_c^2)^2]/\Sigma[w(F_0^2)^2]\}^{1/2}$. $w = 1/[\sigma^2(F_0)^2 + (aP)^2 + bP]$, $P = [\max.(F_0^2, 0) + 2(F_c)^2]/3$, where $a = 0.0379$ and $b = 0.2376$.

atoms, anisotropic thermal parameters for all the non-hydrogen atoms, and isotropic thermal parameters for all the hydrogen atoms. Full-matrix least-squares refinement against $|F^2|$ was carried out using the WinGx package of programs.[32] Details of the structure solution and final refinements for **I** are given in Table 4. CCDC-674214 (**I**) contains the supplementary crystallographic data for this paper. These data can be obtained free of charge from The Cambridge Crystallographic Data Centre via www.ccdc.cam.ac.uk/data_request/cif.

Acknowledgements

S.N. thanks the Department of Science and Technology (DST), Government of India, for the award of a research grant and of the "RAMANNA" fellowship. The authors thank the Council of Scientific and Industrial Research (CSIR), Government of India, for the award of a fellowship (P.M.) and a research grant. The Board of Research on Nuclear Sciences (BRNS), Department of Atomic Energy (DAE), Government of India, is thanked for its support.

[1] a) T. Furusawa, M. Kawano, M. Fujita, *Angew. Chem.* **2007**, *119*, 5819–5821; *Angew. Chem. Int. Ed.* **2007**, *46*, 5717–5719; b) M. Kawano, T. Kawamichi, T. Haneda, T. Kojima, M. Fujita, *J. Am. Chem. Soc.* **2007**, *129*, 15418–15419; c) D. Maspoch, D. Ruiz-Molina, J. Veciana, *Chem. Soc. Rev.* **2007**, *36*, 770–818; d) T. K. Maji, R. Matsuda, S. Kitagawa, *Nat. Mater.* **2007**, *6*, 142–148; e) C. N. R. Rao, S. Natarajan, R. Vaidhyanathan, *Angew. Chem.* **2004**, *116*, 1490–1521; *Angew. Chem. Int. Ed.* **2004**, *43*, 1466–1496; f) M. Eddaoudi, J. Kim, D. Vodak, A. Sudik, J. Wachter, M. O'Keefe, O. M. Yaghi, *Proc. Natl. Acad. Sci. USA* **2002**, *99*, 4900–4904.

[2] a) E. Lee, J. Heo, K. Kim, *Angew. Chem.* **2000**, *112*, 2811–2813; *Angew. Chem. Int. Ed.* **2000**, *39*, 2699–2701; b) L. Pan, H. Liu, X. Lei, X. Huang, D. H. Olson, N. J. Turro, J. Li, *Angew. Chem.* **2003**, *115*, 560–564; *Angew. Chem. Int. Ed.* **2003**, *42*, 542–546; c) X. H. Bu, M. L. Tong, H. C. Chang, S. Kitagawa, S. R. Batten, *Angew. Chem.* **2004**, *116*, 194–197; *Angew. Chem. Int. Ed.* **2004**, *43*, 192–195; d) J. P. Zhang, Y. Y. Lin, X. C. Huang, X. M. Chen, *J. Am. Chem. Soc.* **2005**, *127*, 5495–5506; e) B. Moulton, M. J. Zaworotko, *Chem. Rev.* **2001**, *101*, 1629–1658; f) M. Fujita, M. Tominaga, A. Hori, B. Therrien, *Acc. Chem. Res.* **2005**, *38*, 369–378.

[3] a) T. M. Reineke, M. Eddaoudi, D. Moler, M. O'Keeffe, O. M. Yaghi, *J. Am. Chem. Soc.* **2000**, *122*, 4843–4844; b) L. Pan, K. M. Adams, H. E. Hernandez, X. T. Wang, C. Zheng, Y. Hattori, K. Kaneko, *J. Am. Chem. Soc.* **2003**, *125*, 3062–3067; c) B. Zhao, P. Cheng, X. Y. Chen, C. Cheng, W. Shi, D. Z. Liao, S. P. Yan, Z. H. Jiang, *J. Am. Chem. Soc.* **2004**, *126*, 3012–3013.

[4] J. Huheey, E. A. Keiter, R. L. Keiter, *Inorganic Chemistry: Principles of Structure and Reactivity*, 4th ed., Pearson Education, **2000**.

[5] a) T. M. Reineke, M. Eddaoudi, M. Fehr, D. Kelly, O. M. Yaghi, *J. Am. Chem. Soc.* **1999**, *121*, 1651–1657; b) X. Guo, G. Zhu, Q. Fang, M. Xue, G. Tian, J. Sun, X. Li, S. Qui, *Inorg. Chem.* **2005**, *44*, 3850–3855.

[6] S. Han, J. V. Smith, *Acta Crystallogr. Sect. A* **1999**, *55*, 332–382.

[7] a) A. F. Wells, *Three-Dimensional Nets and Polyhedra*, Wiley, New York, **1977**; b) M. O'Keefe, B. G. Hyde, *Philos. Trans. R. Soc. Lond.* **1980**, *295*, 553–648.

[8] a) J. R. Stork, V. S. Thoi, S. M. Cohen, *Inorg. Chem.* **2007**, *46*, 11213–11223; b) F. Luo, S. R. Batten, Y. Che, J. M. Zheng, *Chem. Eur. J.* **2007**, *13*, 4948–4955; c) P. Mahata, G. Sankar, G. Madras, S. Natarajan, *Chem. Commun.* **2005**, 5787–5789; d) R. J. Hill, D. L. Long, N. R. Champness, P. Hubberstey, M. Schroder, *Acc. Chem. Res.* **2005**, *38*, 337–350; e) S. Furukawa, M. Ohba, S. Kitagawa, *Chem. Commun.* **2005**, 865–867; f) F. Q. Wang, X. J. Zheng, Y. H. Wan, C. Y. Sun, Z. M. Wang, K. Z. Wang, L. P. Jin, *Inorg. Chem.* **2007**, *46*, 2956–2958; g) L. R. MacGillivray, S. Subramanian, M. J. Zaworotko, *J. Chem. Soc. Chem. Commun.* **1994**, 1325–1326.

[9] a) M. Du, X. J. Jiang, X. J. Zhao, *Inorg. Chem.* **2007**, *46*, 3984–3995; b) M. Sarkar, K. Biradha, *Cryst. Growth Des.* **2007**, *7*, 1318–1331; c) M. Fujita, Y. J. Kwon, S. Washizu, K. Ogura, *J. Am. Chem. Soc.* **1994**, *116*, 1151–1152; d) M. Felloni, A. J. Blake, N. R. Champness, P. Hubberstey, C. Wilson, M. Schröder, *J. Supramol. Chem.* **2002**, *2*, 163–174; e) T. J. Won, J. K. Clegg, L. F. Lindoy, J. C. McMurtrie, *Cryst. Growth Des.* **2007**, *7*, 972–979; f) D. R. Turner, J. S. Hattan, S. R. Batten, *CrystEngComm* **2008**, *10*, 34–38.

[10] C. A. Williams, A. J. Blake, P. Hubberstey, M. Schröder, *Chem. Commun.* **2005**, 5435–5437.

[11] A. B. Lysenko, E. V. Govor, H. Krautscheid, K. V. Domasevitch. *Dalton Trans.* **2006**, 3772–3776.

[12] M. Du, Z. H. Zhang, L. F. Tang, X. G. Wang, X. J. Zhao, S. R. Batten, *Chem. Eur. J.* **2007**, *13*, 2578–2586.

[13] a) A. Patra, C. S. Friend, R. Kapoor, P. N. Prasad, *Chem. Mater.* **2003**, *15*, 3650–3655; b) X. Wang, X. Kong, G. Shan, Y. Yu, Y. Sun, L. Feng, K. Chao, S. Lu, Y. Li, *J. Phys. Chem. B* **2004**, *108*, 18408–18413.

[14] a) C. Daiguebonne, N. Kerbellec, K. Bernot, Y. Gerault, A. Deluzet, O. Guillou, *Inorg. Chem.* **2006**, *45*, 5399–5406; b) X. Guo, G. Zhu, Z. Li, Y. Chen, X. Li, S. Qui, *Inorg. Chem.* **2006**, *45*, 4065–4070; c) X. Guo, G. Zhu, F. Sun, Z. Li, X. Zhao, X. Li, H. Wang, S. Qui, *Inorg. Chem.* **2006**, *45*, 2581–2587.

[15] a) B. Zhao, H. L. Gao, X. Y. Chen, P. Cheng, W. Shi, D. Z. Liao, S. P. Yan, Z. H. Jiang, *Chem. Eur. J.* **2006**, *12*, 149–158; b) S. K. Ghosh, P. K. Bharadwaj, *Inorg. Chem.* **2003**, *42*, 8250–8254; c) S. K. Ghosh, P. K. Bharadwaj, *Inorg. Chem.* **2005**, *44*, 3156–3161; d) T. K. Maji, G. Mostafa, H. C. Chang, S. Kitagawa, *Chem. Commun.* **2005**, 2436–2438.

[16] C. Qin, X. L. Wang, E. B. Wang, Z. M. Su, *Inorg. Chem.* **2005**, *44*, 7122–7129.

[17] K. Nakamoto, *Infrared and Raman Spectra of Inorganic and Coordination Compounds*, Wiley-Interscience, New York, **1963**.

[18] a) B. D. Chandler, J. O. Yu, D. T. Cramb, G. K. H. Shimizu, *Chem. Mater.* **2007**, *19*, 4467–4473; b) D. T. de Lill, A. de Bettencourt-Dias, C. L. Cahill, *Inorg. Chem.* **2007**, *46*, 3960–3965.

[19] a) J. C. G. Bunzli, G. R. Choppin, *Lanthanide Probes in Life, Chemical, and Earth Science: Theory and Practice*, Elsevier, Amsterdam, **1989**; b) G. Blasse, B. C. Grabmaier, *Luminescent Materials*, Springer, Berlin, **1994**.

[20] a) B. D. Chandler, D. T. Cramb, G. K. H. Shimizu, *J. Am. Chem. Soc.* **2006**, *128*, 10403–10412; b) P. R. Selvin, *Nat. Struct. Biol.* **2000**, *7*, 730–734; c) R. E. Whan, G. A. Crosby, *J. Mol. Spectrosc.* **1962**, *8*, 315–327.

[21] A. Thirumurugan, S. Natarajan, *J. Mater. Chem.* **2005**, *15*, 4588–4594.

[22] a) C. Serre, F. Pelle, N. Gardant, G. Ferey, *Chem. Mater.* **2004**, *16*, 1177–1182; b) F. Millange, C. Serre, J. Marrot, N. Gardant, F. Pelle, G. Ferey, *J. Mater. Chem.* **2004**, *14*, 642–645; c) C. Serre, F. Millange, N. Thouvenot, N. Gardant, F. Pelle, G. Ferey, *J. Mater. Chem.* **2004**, *14*, 1540–1543.

[23] H. S. Wang, B. Zhao, B. Zhai, W. Shi, P. Cheng, D. Z. Liao, S. P. Yan, *Cryst. Growth Des.* **2007**, *7*, 1851–1857.

[24] a) S. Surble, C. Serre, F. Millange, F. Pelle, G. Ferey, *Solid State Sci.* **2005**, *7*, 1074–1082; b) Z. H. Zhang, T. Okamura, Y. Hasuchika, H. Kawaguchi, L. Y. Kong, W. Y. Sun, N. Ueyama, *Inorg. Chem.* **2005**, *44*, 6219–6227.

[25] J. Yang, Q. Yue, G. D. Li, J. J. Cao, G. H. Li, J. S. Chen, *Inorg. Chem.* **2006**, *45*, 2857–2865.

[26] a) F. Auzel, *C. R. Acad. Sci. Paris* **1966**, 1016–1019; b) J. C. Wright in *Topics in Applied Physics: Radiationless Processes in Molecules and Condensed Phases* (Ed.: F. K. Fong), Springer, Berlin, **1976**.

[27] F. Auzel, *Chem. Rev.* **2004**, *104*, 139–174.

[28] J. J. Ju, T. Y. Kwon, H. K. Kim, J. H. Kim, S. C. Kim, M. Cha, S. I. Yun, *Mater. Lett.* **1996**, *29*, 13–18.

[29] SMART (V 5.628), SAINT (V 6.45a), XPREP, SHELXTL, Bruker AXS Inc., Madison, WI, USA, **2004**.

[30] G. M. Sheldrick, Siemens Area Correction Absorption Correction Program, University of Göttingen, Göttingen, Germany, **1994**.

[31] G. M. Sheldrick, SHELXL97 Program for Crystal Structure Solution and Refinement, University of Göttingen, Göttingen, Germany, **1997**.

[32] J. L. Farrugia, "WinGx Suite for Small-Molecule Single-Crystal Crystallography", *J. Appl. Crystallogr.* **1999**, *32*, 837–838.

Received: February 7, 2008
Revised: April 3, 2008
Published online: May 19, 2008

